Inorganic Chemistry

ARTICLE

pubs.acs.org/IC

Influence of the Nature of the Absorption Band on the Potential Performance of High Molar Extinction Coefficient Ruthenium(II) Polypyridinic Complexes As Dyes for Sensitized Solar Cells

Francisco Gajardo,[†] Mauricio Barrera,[†] Ricardo Vargas,[†] Irma Crivelli,[‡] and Barbara Loeb*[,†]

[†]Facultad de Química, Pontificia Universidad Católica de Chile, Casilla 306, Santiago, Chile

[‡]Facultad de Ciencias, Universidad de Chile, Las Palmeras 3425, Santiago, Chile

Supporting Information

ABSTRACT: When tested in solar cells, ruthenium polypyridinic dyes with extended π systems show an enhanced light-harvesting capacity that is not necessarily reflected by a high (collected electrons)/(absorbed photons) ratio. Provided that metal-to-ligand charge transfer bands, MLCT, are more effective, due to their directionality, than intraligand (IL) $\pi-\pi^*$ bands for the electron injection process in the solar cell, it seems important to explore and clarify the nature of the absorption bands present in these types of dyes. This article aims to elucidate if all the absorbed photons of these dyes are potentially useful in the generation of electric current. In other words, their potentiality as dyes must also be analyzed from the point of view of their contribution to the generation of excited states potentially useful for direct injection. Focusing on the assignment of the absorption bands and the nature of the emitting state, a systematic study for a series of ruthenium complexes with 4,4′-distyryl-2,2′-dipyridine (LH) and 4,4′-bis[p-(dimethylamino)-α-styryl]-2,2′-bipyridine ($LNMe_2$) "chromophoric" ligands was undertaken. The observed experimental results were complemented with TDDFT calculations to elucidate the nature of the absorption bands, and a theoretical model was proposed to predict the available energy that could be injected from a singlet or a triplet excited state. For the series studied, the results indicate that the percentage of MLCT character to the anchored ligand for the lower energy absorption band follows the order $[Ru(deebpy)_2(LNMe_2)](PF_6)_2$ > $[Ru(deebpy)_2(LH)](PF_6)_2$ > $[Ru(deebpy)(LH)_2](PF_6)_2$, where deebpy is 4,4′-bis(ethoxycarbonyl)-2,2′-bipyridine, predicting that, at least from this point of view, their efficiency as dyes should follow the same trend.

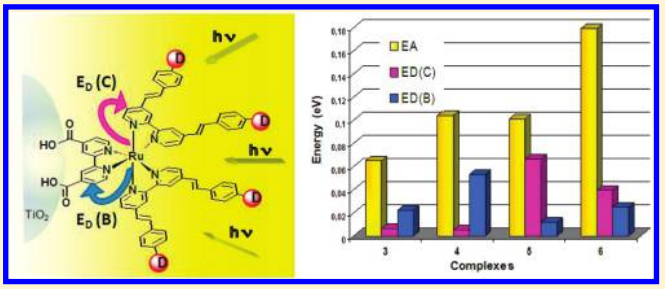

INTRODUCTION

Ruthenium compounds containing monodentate, bidentate, tridentate, and tetradentate pyridinic ligands have been intensely used as dyes in nanocrystalline sensitized solar cells. These pyridinic and polypyridinic ligands can be functionalized by incorporating electron-withdrawing groups (e.g., carboxylate, phosphonate), which at the same time play the role of an anchor group to the TiO_2 semiconductor in the cell.[1] The ruthenium polypyridinic complexes present intense metal-to-ligand charge transfer (MLCT) absorption bands in the visible region,[2] which is one of the factors directly responsible for optimization of the absorption process or LHE (light-harvesting efficiency) of the cell.[3] Thus, an increase in the molar extinction coefficient of this band in the ruthenium dye chromophore is expected to increase the LHE of the cell. This effect in turn could have a positive impact on the IPCE (incident photon to collected electron quantum efficiency) cell parameter and consequently on the photoaction spectra of IPCE (λ) vs λ.[4]

An increase of the capacity of the dye to absorb radiation appears as one of the key factors to improve solar energy conversion to electricity by a solar cell. This aspect can be undertaken either from the point of view of the number of photons absorbed or by the amplitude of the wavelength interval where absorption occurs. On this basis, some ruthenium dyes have been reported presenting "chromophoric polypyridinic ligands", e.g., bipyridinic ligands with an attached extended π-electronic system, Scheme 1.[5] On the other hand, donor groups such as methoxy or substituted amines have been incorporated as substituents on these "chromophoric ligands",[2a,b,6] allowing an increase in absorption.[7] Specifically, a series of ruthenium complexes with ligands of the type 4,4′-distyryl-2,2′-dipyridine have been reported, presenting an increased light-harvesting capacity and a relatively good yield as dyes. In 2006 Grätzel et al. described the requirements for light-harvesting systems, emphasizing the directionality of the charge redistribution produced by light absorption. Experimental results have been reported for the tetrabutylammonium [ruthenium (4-carboxylic acid-4′-carboxylate-2,2′-bipyridine)-(4,4′-di(2-(3,6-dimethoxyphenyl)ethenyl)-2,2′-bipyridine)$(NCS)_2$], N945H, and the fully deprotonated tetrabutylammonium

Received: October 14, 2010
Published: May 31, 2011

   dx.doi.org/10.1021/ic1020862 | *Inorg. Chem.* 2011, 50, 5910–5924

Scheme 1

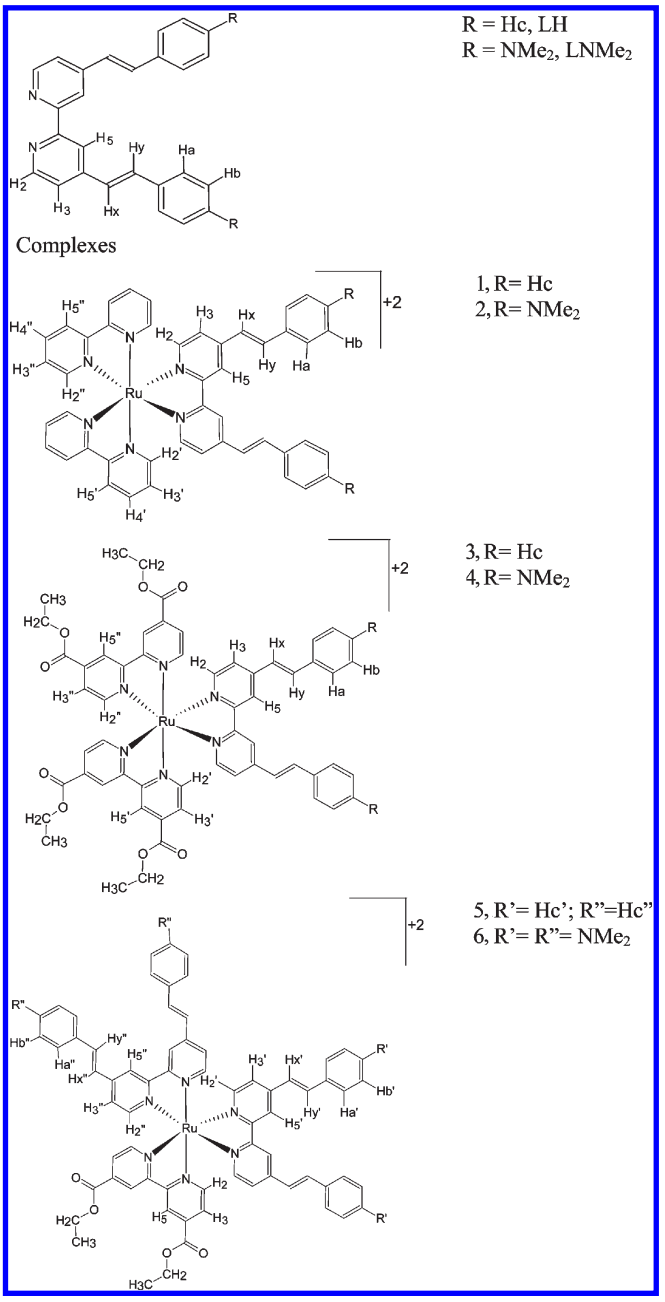

[ruthenium (4,4′-carboxylate-2,2′-bipyridine)(4,4′-di(2-(3-dimethoxyphenyl)-ethenyl)-2,2′-bipyridine)$(NCS)_2$], N945, sensitizers, together with an INDO/DFT modeling of the N945 complex absorbed on TiO_2.[8a] In this report the authors conclude that selective functionalization of a ruthenium complex allows red-shift absorption spectra and an enhanced molar extinction coefficient and, at the same time, creating significant directionality in the excited state.

In spite of the mentioned increased light-harvesting capacity of complexes with these types of "chromophoric ligands", the estimated internal quantum efficiency (ratio of collected electrons to absorbed photons) for these dyes is only 50%, which is lower than expected according to their high absorption.[9] To shed some light into the latter point, it is relevant to determine the nature of the absorption bands, especially in the visible region.[10] Generally, it is accepted that MLCT, due to its directionality, should be effective for electron injection in the semiconductor band, while IL bands should not. Published articles in the literature related to ruthenium complexes with "chromophoric polypyridinic ligands" are not conclusive on assigning the absorption bands, fundamentally for the fact that the IL bands shift to lower energies for donor substituents in the ligand.[11] In this case, the energy of the IL band may come close to the energy level of the MLCT band and even produce a crossing between these two levels, making difficult an assignment by a simple correlation with the spectrum of $[Ru(bpy)_3]^{2+}$-type complexes.[12]

Regarding another experimental variable, Filippo De Angelis et al. published a manuscript about the influence of the sensitizer adsorption mode on the open-circuit potential of dye-sensitized solar cells. In order to understand the origin of such experimental observations, they performed DFT calculations to obtain information on the dipole moments in the geometry and orientation corresponding to the free and adsorbed dye for the different isomers of $(Bu_4N)_2[Ru(dcbpyH)_2(NCS)_2]$, N719, and $[Ru(dcbpyH_2)(tdbpy)(NCS)_2]$, N621, sensitizers, with dcbpy = 2,2′-bipyridyl-4,4′-dicarboxylato, $dcbpyH_2$ = (4,4′-dicarboxylic acid-2,2′-bipyridine), and tdbpy = 4,4′-ditridecyl-2,2′-bipyridine.[8b] Also reported was the relation of the magnitude and orientation of dipolar fields with the different adsorption modes and with the value of the open-circuit voltage.

Finally, the injection capacity of the dye is also an important variable to be considered in a solar cell. This injection may occur from a Franck−Condon "hot" excited state or, more probable, from the thermally equilibrated "thexi" state. For a ruthenium complex with polypyridinic ligands, the latter is probably the lowest lying excited triplet state.

The present article aims to elucidate whether the absorbed photons by this variety of dyes with "chromophoric ligands" are potentially useful in the generation of electric current. Focusing on the assignment of the absorption bands of this sort of complexes, a systematic study using spectroscopic as well as electrochemical tools was undertaken. Also examined was the effect of the presence of donor substituents in the chromophoric ligands on the relative position of the MLCT and the IL bands. The observed experimental results were analyzed with theoretical calculations.[13] Specifically, the nature of the electronic transitions was examined by simulating their electronic spectra with TDDFT methods and calculating the transition density change within the molecule when an electronic transition occurs. An electron density fragment analysis was performed, in order to understand the electronic density distribution in the different ligands, both for the first excited singlet and for the first excited triplet states. The direct injection capacity of these states was analyzed based on the electronic density on the ligand directly anchored to the semiconductor surface.

To achieve this goal, a series of ruthenium complexes bearing "chromophoric ligands" of the type 4,4′-distyryl-2,2′-dipyridine, LH, and 4,4′-bis[*p*-(dimethylamino)-α-styryl]-2,2′-bipyridine, $LNMe_2$, was synthesized. The ligands and the corresponding complexes are depicted in Scheme 1. A comparison of different pairs of complexes allows analyzing the effect of different factors. Specifically, by comparing complexes $[Ru(bpy)_2(LH)](PF_6)_2$ (**1**) and $[Ru(bpy)_2(LNMe_2)](PF_6)_2$ (**2**) or $[Ru(deebpy)_2(LH)](PF_6)_2$ (**3**) and $[Ru(deebpy)_2(LNMe_2)](PF_6)_2$ (**4**) the effect of the donor NMe_2 group on the nature of the lowest energy band was analyzed. On the other hand, by comparing complexes **3** and

dx.doi.org/10.1021/ic1020862 |*Inorg. Chem.* 2011, 50, 5910–5924

$[Ru(deebpy)(LH)_2](PF_6)_2$ (**5**) or **4** and $[Ru(deebpy)(LNMe_2)_2](PF_6)_2$ (**6**) the presence of the anchoring carboxylate groups on the electronic nature of the complexes was analyzed. Also studied were the spectroscopic properties of complexes **5** and **6** with an increased number of chromophoric ligands attached to the ruthenium center. As mentioned, the character of the absorption band was elucidated by means of TDDFT-type calculations, and the predominance of the MLCT absorption to the anchoring bpy ligand as well as a high electronic concentration in this ligand in the excited S and T were related to a probable higher efficiency as a solar cell dye.

EXPERIMENTAL SECTION

Analytical Methods. *UV−Vis and Emission Spectroscopy.* UV−vis absorption measurements were made on a Shimadzu UV 3101PC spectrophotometer. Photoluminescence (PL) spectra were recorded on a Perkin-Elmer LS5 spectrofluorophotometer.

Infrared Spectroscopy. Infrared (IR) spectra for the desired compounds and reactants were recorded as KBr mulls in a Bruker Vector 22 FTIR spectrometer.

Elemental Analysis and Mass Spectrometry. Elemental analysis was performed on a Fisons Instrument Analyzer, model EA1108/CHNS-O with PC NCR system 3225. Mass spectra were recorded with an LCQ Duo Ion Trap Mass Spectrometer (Thermo Finnigan, USA).

NMR Spectroscopy. ^{1}H NMR spectra were recorded on a Bruker ACL 200 200 MHz spectrometer with tetramethylsilane, $Si(CH_3)_4$, as the reference or on a Bruker AVANCE 400 FT-NMR spectrometer.

Electrochemistry. Cyclic voltammetry was performed in nitrogen-saturated 0.1 M tetrabutylammonium hexafluorophosphate ($TBAPF_6$) as supporting electrolyte in CH_3CN. A BAS model CV50w potentiostat was used in a standard three-electrode arrangement with a Pt or glassy platinum working electrode, a Pt gauze counter electrode, and a Ag/AgCl reference electrode. All potentials are referred with respect to this last electrode.

Materials. Reagents and solvents were purchased from Aldrich and used without further purification. The syntheses of the 4,4′-dicarboxylic acid-2,2′-bipyridine (dcbpy)[14] and 4,4′-bis(ethoxycarbonyl)-2,2′-bipyridine (deebpy)[15] ligands and of the $[Ru(bpy)_2Cl_2]\cdot 2H_2O$ and $[Ru(deebpy)_2Cl_2]\cdot 2H_2O$ complexes were carried out according to procedures described in the literature.[16]

Computational Details. *General.* All calculations were performed with the ADF package.[17] Geometrical optimizations were carried out under C_2 symmetry using the PW91[18] exchange correlation functional, which was selected among other functionals (LDA,[19] BP86,[20] BLYP) to best reproduce the $[Ru(bpy)_3]^{2+}$ crystalline structure. The standard DZP[21] basis set was employed for elements of the first series (C, N, O, H), while for ruthenium a TZP[21] basis set was chosen. TDDFT/ALDA calculations were also performed for the ligands and metal complexes, employing the PBE[22] exchange correlation and a ZORA TZ2P[21] basis set for ruthenium. A solvent effect study (acetonitrile) was included only for complexes through the COSMO model where the shape of the cavity is defined with a Klamt surface. Only the first 70 excitations were considered. The PBE exchange functional was selected after checking others (LDA, BLYP, PW91, OLYP,[23] LB94[24]) for being the one that best matches experimental spectra for the complexes under study. Triplet energies were calculated using the ΔSCF method. In order to interpret the emission bands, the difference in total energy was determined in terms of two independent calculations, one for the energy of the molecule at the optimized geometry in the first triplet state configuration and the other for the molecule in the ground state, although at the mentioned optimized geometry obtained for the triplet state. All triplet state geometries were obtained through an unrestricted calculation employing the PBE exchange functional. Optimized geometries were checked to be at an energy minimum by performing vibrational frequencies calculations and verifying that only real frequencies were present. Solvations effects were also included by means of the COSMO model.

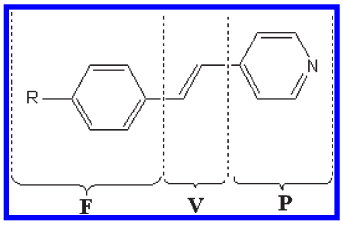

Figure 1. Decomposition of the chromophoric ligand in terms of orthogonal fragments.

Fragment Analysis. Because the 4,4′-distytyl-2,2′-dipyridine-type ligands show a C_2 symmetry they can be analyzed considering one-half of it. Additionally, it is possible to define three kinds of orthogonal fragments, F, V, and P, Figure 1. The fragment F contains the para-substituted phenyl ring, fragment V is centered on the vinyl moiety, and P corresponds to the pyridine ring.

The same scheme was applied for the complexes under study: the C_2 symmetry enables one to decompose the whole structure in terms of five orthogonal fragments; the first two are centered on the substituted bipyridine and on the ruthenium atom. The remaining three fragments are located on the chromophoric ligand and follow the decomposition mentioned above. Through this approach it is possible to assign a character to each molecular orbital in accordance to the predominant fragment(s), leading to classifying them as metallic (M) or centered on bipyridine (B), on the dimethyl ester of bipyridine (Bp), or on the chromophoric ligands (C).

Transition Density Analysis. Molecular orbitals (MO) can be decomposed in terms of a linear combination of orthogonal fragments, each of them related to a specific group of atoms with chemical meaning (ligand, substituent, or metal)

$$\Psi_i = \sum_{\alpha=1}^{n_g} c_{\alpha,i} g_\alpha \tag{1}$$

with

$$\sum_{\alpha=1}^{n_g} c_{\alpha,i}^2 = 1 \text{ and } \langle g_\alpha | g_\beta \rangle = 0 \ \forall \ \alpha \neq \beta \tag{2}$$

It follows that the probability of finding an electron on molecular orbital Ψ_i over fragment g_α is c_α^2; in this sense, each MO can be characterized according to the fragment that prevails, corresponding to the fragment with highest c_α^2.

On the other hand, a single excitation (γ) involving two molecular orbitals can be defined. One of these MOs, Ψ_H, arises from the ground state (GS) and the other, Ψ_L, from the excited state (ES). Accordingly, the process $\Psi_H \rightarrow \Psi_L$ will correspond to a displacement of electronic density from the fragment $\{g_\alpha\}$ of Ψ_H to the fragment $\{g_\beta\}$ of Ψ_L in accordance with the process $\gamma_{\alpha\beta}$: $g_\alpha \rightarrow g_\beta$ or within the same fragment $g_\alpha \rightarrow g_\alpha$ with $\alpha,\beta = \{F,V,P,M,C,B,Bp\}$.

Additionally, an electronic transition, Γ_λ, can be visualized as the sum of a series of single electronic excitations occurring at wavelength λ with energy $h\nu$ and probability of occurring measured by the oscillator strength f_λ. Hence

$$\Gamma_\lambda = f_\lambda \left(\sum_{k=1}^{nk} d_{k,\lambda} \gamma_{\alpha\beta} \right) \tag{3}$$

where $d_{k,\lambda} > 0$ and $\Sigma_k d_{k\lambda} = 1$, which ensures that it is a one-photon absorption process.

dx.doi.org/10.1021/ic1020862 |*Inorg. Chem.* 2011, 50, 5910–5924

Also, for the electronic transition occurring on the wavelength range $[\lambda_i, \lambda_f]$ it is possible to define a distribution function $\zeta(\alpha,\beta)$ showing how a specific excitation, $\alpha \rightarrow \beta$, contributes along the overall interval of wavelengths

$$\zeta(\alpha,\beta) = \left(\sum_{\lambda} f_\lambda (d_{k,\lambda}\gamma_{\alpha\beta})/\sum_{\lambda}\Gamma_\lambda\right) \text{ for } \lambda \in [\lambda_i,\lambda_f] \quad (4)$$

Furthermore, the energy transferred from all transitions to the fragment g_β is calculated through

$$E(g_\beta) = E_A \sum_{\beta} \zeta(\alpha,\beta) \quad (5)$$

where E_A is the absorbed energy obtained from

$$E_A = f_{max}\Delta\nu \text{ with } \Delta\nu = hc/(\lambda_f - \lambda_i) \quad (6)$$

Until now, the analysis has been mainly focused on the absorbed energy. Nevertheless, by means of intersystem crossing (singlet to triplet) the injection process may occur from different electronic states with respect to those involved in the Franck−Condon absorption. Equation 7 permits one to calculate $I_T(g_\beta)$, the amount of energy that can be delivered from fragment g_β into the T_1 state

$$I_T(g_\beta) = E(g_\beta)\varphi_T(g_\beta) \quad (7)$$

In this equation $E(g_\beta)$ is calculated from eq 5 and $\varphi_T(g_\beta)$ is a distribution function with a maximum value of one, which contains information about the participation of the different fragments in the state under study. Data for this function is obtained through a fragment population analysis.[25]

Synthesis. *4,4′-Bis(2-hydroxy-2-phenyl)ethyl-2,2′-bipyridine and 4,4′-Bis[2-hydroxy-2-p-(dimethylaminophenyl)ethyl]-2,2′-bipyridine.* These syntheses were carried out as described in the literature[26] using benzaldehyde and *p*-toluoldehyde, respectively.

4,4′-Distyryl-2,2′-bipyridine, LH. A 602 g (1.52 mmol) amount of the diol and 60 mL of acetic acid are combined. The resulting mixture is heated to reflux for 18 h. Later, the solution is allowed to cool, preventing the acetic acid from freezing. The formed solid is separated by filtration and washed with ethyl ether. Yield: 65%. IR, KBr (cm^{-1}): $\nu_{C-H\ Aromatic}$ = 3027. ^{1}H NMR ($CDCl_3$) δ (ppm): 8.69 (d, 1H, H2), 8.55 (s, 1H, H5), 7.58 (d, 2H, Ha), 7.47 (d, 1H, Hx), 7.40 (t, 3H, Hb, Hc), 7.34 (d, 1H, H3), 7.15 (d, 1H, Hy). Anal. Calcd for $C_{26}H_{20}N_2$: C, 86.64; H, 5.59; N, 7.77. Found: C, 86.39; H, 5.63; N, 7.74.

4,4′-Bis[p-(dimethylamino)-α-styryl]-2,2′-bipyridine, $LNMe_2$. The synthetic procedure is carried out just as described by A. Juris.[26] IR, KBr (cm^{-1}): $\nu_{C-H\ Aromatic}$ = 3021, ν_{C-N} = 1360. ^{1}H NMR ($CDCl_3$) δ (ppm): 8.60 (d, J = 5.1 Hz, 1H, H2), 8.46 (s, 1H, H5), 7.45 (d, J = 8.8 Hz, 2H, Ha), 7.39 (d, J = 16.2 Hz, 1H, Hx), 7.33 (dd, J^1 = 5.1 Hz, J^2 = 1.6 Hz, 1H, H3), 6.91 (d, J = 16.2 Hz, 1H, Hy), 6.71 (d, J = 8.34 Hz, 2H, Hb), 2.99 (s, 6H, N−$(CH_3)_2$). Anal. Calcd for $C_{30}H_{30}N_4 \cdot 0.5H_2O$: C, 79.07; H, 6.86; N, 12.29. Found: C, 79.07; H, 6.89; N, 12.38.

[Ru(bpy)$_2$(LH)](PF$_6$)$_2$, ***1***. The synthetic procedure is carried out as described by B. P. Sullivan.[27] A 69.3 mg (0.192 mmol) amount of LH and 97.2 mg (0.384 mmol) of $AgPF_6$ are dissolved in 25 mL of ethanol. To the resulting mixture, 100 mg (0.192 mmol) of $Ru(bpy)_2Cl_2 \cdot 2H_2O$ is added. Then, the mixture is heated to reflux for 6 h, shielding the system from light by aluminum foil. Afterward, the mixture is filtered over Celite and a stoichiometic quantity of NH_4PF_6 is added to the remaining fluid. The formed solid is filtered under vacuum and purified by column chromatography over aluminum oxide using ethanol followed by acetone. The acetone portion is concentrated and collected on ethyl ether. Yield: 68%. IR, KBr (cm^{-1}): $\nu_{C-H\ Aromatic}$ = 3082, ν_{P-F} = 840, 557. ^{1}H NMR ($(CD_3)_2CO$) δ (ppm): 9.05 (s, 2H, H5), 8.79 (d, 4H, H2′, H2″), 8.18 (t, 4H, H3′, H3″), 8.14 (d, 2H, H5″), 8.03 (d, 2H, H5′), 7.90 (d, 2H, H2), 7.80 (d, 2H, Hx), 7.70−7.68 (m, 6H, H3, Ha), 7.56 (dd, 4H, H4′, H4″), 7.43 (d, 2H, Hy), 7.42−7.34 (m, 6H, Hb, Hc). Anal. Calcd for $C_{46}H_{36}N_6RuF_{12}P_2 \cdot 0.5H_2O$: C, 51.50; H, 3.48; N, 7.83. Found: C, 51.45; H, 3.89; N, 7.85.

[Ru(bpy)$_2$(LMe$_2$)](PF$_6$)$_2$, ***2***. The synthetic procedure is identical to that described for **1**. Yield: 74%. IR, KBr (cm^{-1}): $\nu_{C-H\ Aromatic}$ = 3085, $\nu_{C-H\ Aliphatic}$ = 2920, ν_{N-C} = 1364, ν_{P-F} = 842, 558. ^{1}H NMR ($(CD_3)_2CO$) δ (ppm): 8.86 (s, 2H, H5), 8.77 (d, 4H, H2′, H2″), 8.17−8.12 (m, 6H, H3′, H3″, H5″), 8.00 (d, 2H, H5′), 7.74 (d, 2H, H2), 7.63 (d, 2H, Hx), 7.58−7.48 (m, 10H, Ha, H3, H4′, H4″), 7.07 (d, 2H, Hy), 6.74 (d, 4H, Hb), 2.99 (s, 12H, N$(CH_3)_2$). Anal. Calcd for $C_{50}H_{46}N_8RuF_{12}P_2 \cdot H_2O$: C, 51.42; H, 4.14; N, 9.59. Found: C, 51.71; H, 4.21; N, 9.63.

[Ru(deebpy)$_2$(LH)](PF$_6$)$_2$, ***3***. A 100 mg (0.27 mmol) amount of LH was dissolved in 40 mL of hot benzene. In a second round flask, 214 mg (0.27 mmol) of $Ru(deebpy)_2Cl_2$ and 140 mg (0.55 mmol) of $AgPF_6$ were dissolved in DMF. The latter mixture was added dropwise to the LH ligand solution. Then, the mixture was heated to reflux for 6 h, and then the system was allowed to cool to room temperature and the solvent removed under vacuum. The formed solid was dissolved in acetone and filtered on Celite. The filtrate was concentrated and collected over cold hexane. The collected solid was filtered and washed with ethyl ether. IR, KBr (cm^{-1}): $\nu_{C-H\ Aromatic}$ = 3000−3083, $\nu_{C=O}$ = 1728, ν_{P-F} = 839. ^{1}H NMR (CD_3CN) δ (ppm) 9.07 (d, 2H, H2′, H2″), 8.70 (s, 1H, H5), 8.02 (d, 1H, H2), 7.91−7.83 (m, 2H, H3′, H3″), 7.78 (d, 1H, Hx), 7.68 (d, 2H, H5′, H5″), 7.54 (d, 2H, Ha), 7.46 (t, 3H, Hb, Hc), 7.41 (d, 1H, H3), 7.31 (d, 1H, Hy), 4.44 (q, 4H, OCH_2CH_3), 1.38 (t, 6H, OCH_2CH_3). Anal. Calcd for $C_{58}H_{52}N_6O_8RuF_{12}P_2$: C, 51.52; H, 3.88; N, 6.22. Found: C, 51.39; H, 3.90; N, 6.20. *m/z*: 1208 ($M^+ - PF_6^-$); 531 ($M^+ - 2PF_6^-$).

[Ru(deebpy)$_2$(LNMe$_2$)](PF$_6$)$_2$, ***4***. The synthetic procedure was identical to that described for **3**. Yield: 70%. IR, KBr (cm^{-1}): $\nu_{C-H\ Aromatic}$ = 3121, $\nu_{C-H\ Aliphatic}$ = 2863, $\nu_{C=O}$ = 1727, ν_{C-N} = 1384, ν_{P-F} = 840, 558. ^{1}H NMR ($(CD_3)_2CO$) δ (ppm): 9.27 (s, 2H, H5′, H5″), 8.92 (s, 1H, H5), 8.40 (d, 1H, H2), 8.33 (d, 2H, Hb), 8.00 (d, 1H, H3), 7.90 (d, 2H, Ha), 7.69 (d, 1H, Hx), 7.50 (d, 1H, H2′), 7.44 (d, 1H, H2″), 7.07 (d, 1H, Hy), 6.72 (d, 1H, H3′), 6.63 (d, 1H, H3″), 4.41 (m, 4H, OCH_2CH_3), 2.98 (s, 6H, N$(CH_3)_2$), 1.33 (t, 6H, OCH_2CH_3). Anal. Calcd for $C_{62}H_{62}N_8O_8RuF_{12}P_2 \cdot 0.7H_2O$: C, 51.33; H, 4.4; N, 7.72. Found: C, 51.32; H, 4.48; N, 7.75.

[Ru(LH)$_2$Cl$_2$] and [Ru(LNMe$_2$)$_2$Cl$_2$]. This synthetic procedure is carried out similarly to that described by Sullivan,[16] mixing 250 mg (0.69 mmol) of ligand LH, 71 mg (0.27 mmol) of $RuCl_3 \cdot 3H_2O$, 38 mg (0.36 mmol) of hydroquinone, and 470 mg (11.1 mmol) of LiCl in 100 mL of absolute ethanol and then heating to reflux for 8 h. Afterward, the mixture is allowed to cool to room temperature. The remaining solid is filtered under vacuum and washed with small portions of ethyl ether. For complex $[Ru(LNMe_2)_2Cl_2]$ the same procedure is carried out, using 950 mg (2.13 mmol) of ligand $LNMe_2$, 280 mg (1.06 mmol) of $RuCl_3 \cdot 3H_2O$, 140 mg (1.29 mmol) of hydroquinone, and 450 mg (10.6 mmol) of LiCl.

[Ru(deebpy)(LH)$_2$](PF$_6$)$_2$, ***5***. A 67 mg (0.22 mmol) amount of deebpy is added to 20 mL of methanol. In a second round flask, 200 mg (0.22 mmol) of $[Ru(LH)_2Cl_2]$ and 113 mg (0.44 mmol) of $AgPF_6$ in 25 mL of methanol are added dropwise to the deebpy solution. The mixture is heated to reflux for 3 h. Later, the mixture is allowed to reach room temperature and all the solvent is evaporated. The resulting solid is dissolved in acetone and filtered on Celite. The filtrated portion is concentrated and added dropwise to ethyl ether. The resulting solid is removed by filtration under vacuum and washed with ethyl ether. IR, KBr (cm^{-1}): $\nu_{C-H\ Aromatic}$ = 3028−3057, $\nu_{C=O}$ = 1727, ν_{P-F} = 840. ^{1}H NMR (CD_3CN) δ (ppm): 9.03 (s, 1H, H5′), 8.74 (d, 2H, H2, H2″), 8.04 (d, 1H, H2′), 7.83 (d, 1H, H3′), 7.75 (d, 2H, Hx′, Hx″), 7.73 (s, 2H, H5, H5″), 7.67 (d, 4H, Ha′, Ha″), 7.53−7.38 (m, 8H, H3, H3″, Hb′, Hb″, Hc′, Hc″), 7.30 (d, 2H, Hy′, Hy″), 4.42 (q, 2H, OCH_2CH_3), 1.39 (t, 3H, OCH_2CH_3). Anal. Calcd for $C_{68}H_{56}N_6O_4RuF_{12}P_2$: C, 57.83;

dx.doi.org/10.1021/ic1020862 |*Inorg. Chem.* 2011, 50, 5910–5924

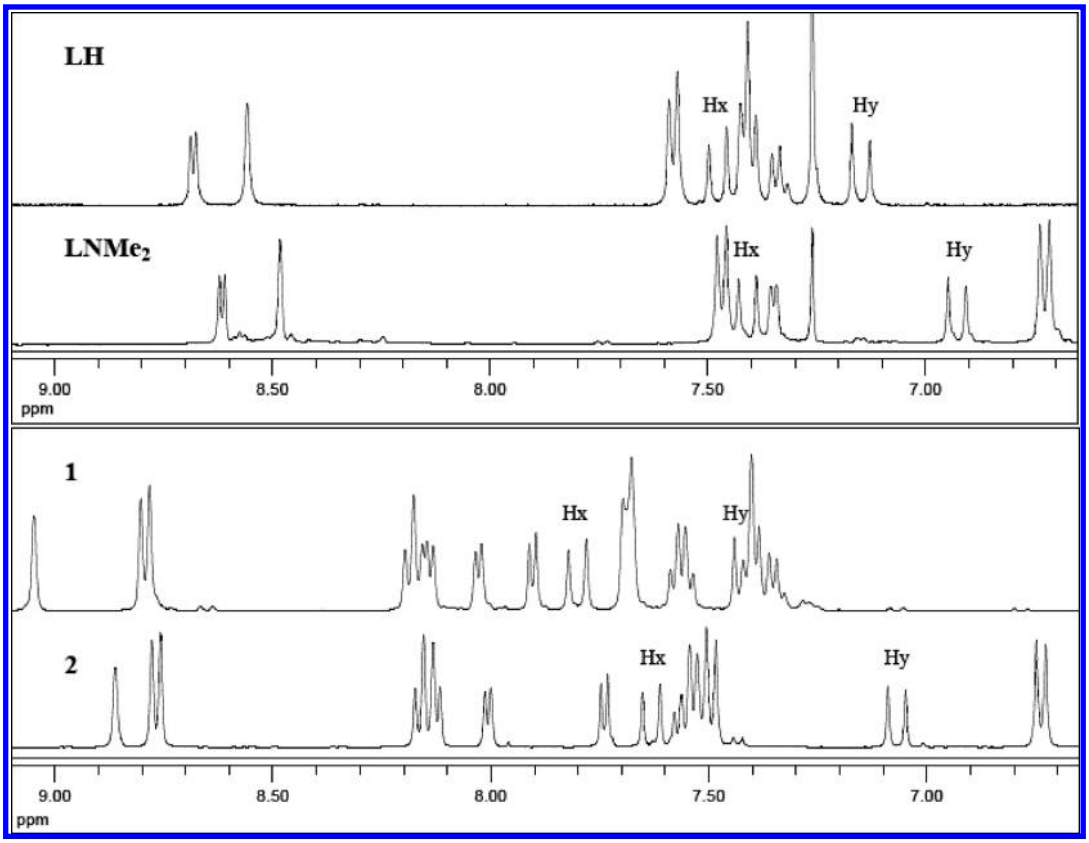

Figure 2. ^{1}H NMR spectra for ligands LH and $LNMe_2$ in ($CDCl_3$) and complexes **1** and **2** in ($(CD_3)_2CO$).

H, 4.00; N, 5.95. Found: C, 57.63; H, 4.03; N, 5.93. *m/z*: 1268.8 ($M^+ - PF_6^-$); 562 ($M^+ - 2PF_6^-$)

[Ru(deebpy)(LNMe$_2$)$_2$](PF$_6$)$_2$, ***6***. An 85 mg (283 mmol) amount of deebpy is dissolved in 10 mL of DMF, and a suspension of 300 mg (282 mmol) of $[Ru(LNMe_2)_2Cl_2]$ in 40 mL of DMF is added. To the resulting mixture, 142 mg (562 mmol) of $AgPF_6$ is added. The mixture is heated to reflux for 6 h and protected from light. Then, the hot mixture is filtered through Celite and the filtrate solution evaporated. The remaining solid is dissolved in acetone and precipitated in ethyl ether. Yield: 74%. IR, KBr (cm^{-1}): $\nu_{C-H\ Aromatic}$ = 3026, $\nu_{C-H\ Aliphatic}$ = 2987, 2923, 2853, $\nu_{C=O}$ = 1723, ν_{N-C} = 1365, ν_{P-F} = 840, 558. ^{1}H NMR (CD_3CN) δ (ppm): 8.99 (s, 2H), 8.62 (s, 3H,), 8.06 (t, 2H), 7.86 (d, 2H), 7.73 (m, 5H), 7.57 (m, 7H), 7.31 (m, 11H), 6.92 (m, 10H), 4.42 (m, 4H, OCH_2CH_3), 3.01 (s, 24H, $N(CH_3)_2$), 1.38 (t, 6H, OCH_2CH_3). Anal. Calcd for $C_{76}H_{76}N_{10}O_4RuF_{12}P_2 \cdot H_2O$: C, 56.96; H, 4.91; N, 8.74. Found: C, 57.13; H, 5.10; N, 8.71.

RESULTS AND DISCUSSION

The IR spectra, taken in KBr, have characteristic bands for the carboxylic groups between 1719 and 1730 cm^{-1} as well as bands belonging to the PF_6^- ion at 558 and 840 cm^{-1}. For complexes **2**, **4**, and **6**, a band at 1364 cm^{-1} is assigned to the stretching of the C−N bond of the donor NMe_2 group. The elemental analyses for these compounds are in agreement with the proposed structures. In compounds such as **3** and **5**, where some deviation was observed, mass spectra permitted confirming the presence of the proposed complex.

Electronic Density Distribution. The ^{1}H NMR spectra for ligands LH and $LNMe_2$ and complexes **1** and **2**, Figure 2, show the electron-donor character of the NMe_2 substituent in the chromophoric ligand. Specifically, the position of the two signals assigned to the Hx and Hy vinyl protons (see proton labeling in Scheme 1) is sensitive to the presence of the amino groups. A chemical shift to higher field is observed for ligand $LNMe_2$, with a difference of 0.08 ppm for Hx and 0.24 ppm for Hy with respect to analogous signals from these protons in the LH ligand spectrum. Similarly, in complex **2** the signals of the Hx and Hy protons are shifted to higher field compared to complex **1**. The shift of the signals is more significant for the complexes than for the ligands. The higher shielding of the protons in the vinyl (V) fragment for $LNMe_2$ and its complexes, compared to LH, correlates well with a higher percentage of electronic density in this fragment in the HOMO orbital, as discussed below (see, e.g., UV−vis spectra section).

Figure 3 summarizes the results of molecular orbital calculations displayed from Tables S1−S6 (Supporting Information). The information is shown by means of molecular orbital energy diagrams for each of the ruthenium complexes under study. A rather different behavior is observed for complexes containing the LH ligand (**1**, **3**, and **5**) when compared to analogous complexes with the $LNMe_2$ ligand (**2**, **4**, and **6**). For example, in complex **1** the five occupied molecular orbitals of higher energy contain pure d metal orbitals and mixtures of d orbitals with π orbitals from the chromophoric ligand. The first six unoccupied molecular orbitals are dominated by those arising from the LUMOs of the bipyridine ligands and the chromophoric ligand. Electronic density analysis shows that the LUMO is localized on the P fragment (Figure 1) of the chromophoric ligand; the LUMO+1 is found 0.11 eV higher in energy and is localized in the bipyridine ligand. As expected, the presence of an

dx.doi.org/10.1021/ic1020862 |*Inorg. Chem.* 2011, 50, 5910–5924

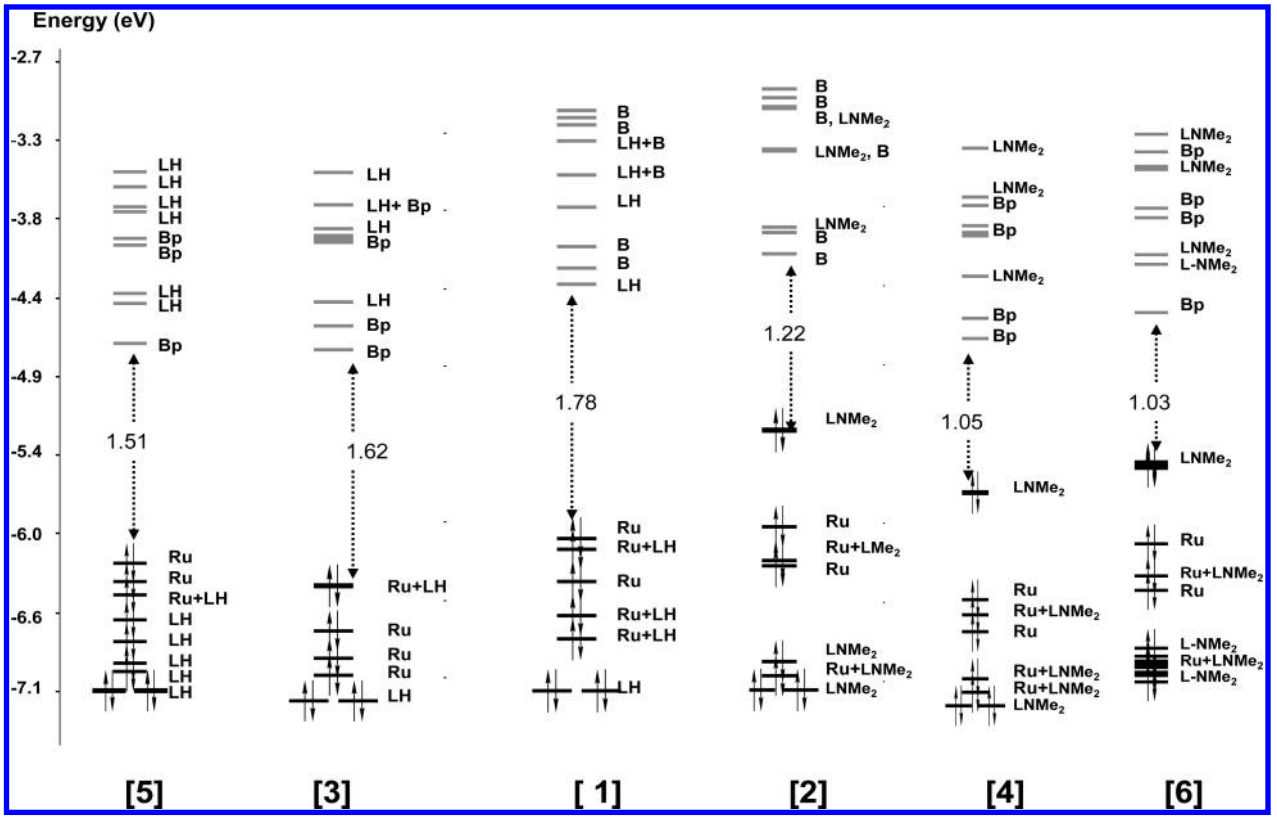

Figure 3. Molecular orbital diagram for ruthenium complexes (Ru = ruthenium; B = bipyridine; Bp = dimethyl dicarboxylate of bipyridine; LH = 4,4′-distyryl-2,2′-dipyridine; $LNMe_2$ = 4,4′-bis[*p*-(dimethylamino)-α-styryl]-2,2′-bipyridine).

electron-withdrawing group, such as −COOMe, in the bipyridine ligand causes a lowering in the energy of the levels, mainly in the MO where this ligand participates. As a consequence, in complexes **3** and **5** the LUMO is centered on the bipyridine orbitals, Bp, with a lower energy than that in the chromophoric ligand orbitals, LH. On the other hand, when the electron-donating dimethylamino substituent is introduced in the para position of the phenyl ring of the chromophoric ligand, as in ligand $LNMe_2$, the opposite effect is observed: all levels show an increase in energy. The effect is particularly notable for complex **2**, while it seems to be attenuated in complexes **4** and **6**, where an anchoring carboxylate acceptor group is present on the bipyridine ligands.

Regarding the HOMO for complex **1**, it shows two nearly degenerated orbitals: one centered on the metal, resulting from a combination of d orbitals ($d_{xy} + d_{x2-y2} + d_{z2}$), and the other a mixture of the $d_{xz} + d_{yz}$ orbitals with a π orbital from the chromophoric ligand. A similar composition is also found for all complexes containing the LH ligand and is independent of the substituent in the bipyridine ligand. The energy of the corresponding HOMOs varies between −6.0 and −6.5 eV. However, when the dimethylamino substituent is introduced, the energy of the HOMO in complexes **2**, **4**, and **6** is raised above −5.8 eV (Tables S2, S4, and S6 in the Supporting Information). This value is the result of the competition between the electron-attracting effect of the substituted bipyridines and the effect of the electron-donor substituent on the chromophoric ligand. The electron density distribution of the HOMO is also altered, being mainly located on the F fragment of the chromophoric ligand, while the HOMO−LUMO band gap of these complexes is reduced about 40% with respect to the corresponding complexes with no amino substitution. Table 1 summarizes the preceding analysis. As mentioned, the effect of the donor NMe_2 substituents on the choromophoric ligand and that of acceptor carboxylate substituents on the bpy ligands is reflected in the nature of the HOMO on the nature of the LUMO and on the energy difference between them, ΔE.

The electrochemical experimental results for the complexes show consistency with the theoretical MO calculations. Table 2 shows the oxidation−reduction potentials for the series of complexes, measured by cyclic voltammetry. It is noteworthy that a correlation coefficient of 0.95 is found when comparing the first electrochemical oxidation potential with the calculated energy of the HOMO orbital for the series of complexes under study. This relationship emerges from Kohn−Sham theory,[28] which states in its exact formulation[29] that the frontier eigenvalue is the ionization potential.[30] However, since solvent effects are included in the present calculations, a correlation between the HOMO eigenvalue and the first oxidation potential is expected. This relationship opens the possibility to employ theoretical information to gain insight on the trend of electrochemical experimental results.

Specifically, looking at the experimental data in Table 2, it can be observed that an irreversible oxidation occurs at 449, 488, and 459 mV for complexes **2**, **4**, and **6**, respectively. These potentials are absent in compounds **1**, **3**, and **5** and are therefore attributed to oxidation of the amino group.[13a] From the MO results in Figure 3 and Table 1, this assumption can be corroborated as complexes **2**, **4**, and **6** possess a HOMO orbital, related to the first oxidation, centered on the dimethylamino group. The same result is obtained by a fragment analysis performed in the same

dx.doi.org/10.1021/ic1020862 |*Inorg. Chem.* 2011, 50, 5910–5924

Table 1. Substituent[a] Effect on the Energy of Frontier Molecular Orbitals for Complexes 1−6

complex	1	2	3	4	5	6
L (chromophoric ligand)	LH	$LNMe_2$	LH	$LNMe_2$	LH	$LNMe_2$
R (for R-bpy)	H	H	COOEt	COOEt	COOEt	COOEt
HOMO centered on	Ru	L	Ru-L	L	Ru	L
LUMO centered on	L	bpy	bpy	bpy	bpy	bpy
Δ(HOMO−LUMO) (eV)	1.78	1.22	1.62	1.05	1.51	1.03
overall substituent effect[b] on the Δ(HOMO−LUMO) gap		HOMO and LUMO destabilized	HOMO and LUMO stabilized	HOMO destabilized LUMO stabilized	HOMO and LUMO stabilized	HOMO destabilized LUMO stabilized

[a] Substituents: Donor NMe_2 group on the chromophoric ligand and COOEt the acceptor group on bpy. [b] Referred to the fully unsubstituted complex **1**.

Table 2. Electrochemical Data of the Complexes[a]

complexes	E_{pa} (mV) [b]	$E_{1/2}$ ($Ru^{2+/3+}$) (mV) [c]	ΔE_p ($Ru^{2+/3+}$) (mV) [d]
1		931	59
2	449	1013	145
3		1115	89
4	488	1151	282
5		968	55
6	459	1232[e]	

[a] Cyclic voltammograms were taken in a 1×10^{-4} M solution of the complex at a sweep rete of 100 mV/s in dry CH_3CN containing 0.1 M tetrabutylammonium hexaflourophosphate as supporting electrolyte (working electrode, disc Pt; reference electrode, Ag/Ag^+, and counter electrode, Pt). [b] Oxidation of substituents. [c] $E_{1/2} = 1/2(E_{pa} + E_{pc})$. [d] $\Delta E_p = |E_{p,c} - E_{p,a}|$. [e] E_{pc}.

way as described before for the free ligand. The second oxidation potential in these complexes is centered on the metal and appears at values similar to those from the first oxidation potential of complexes **1**, **3**, and **5**.

From the ΔE_p ($Ru^{2+/3+}$) values of Table 2, it can be inferred that complexes **1**, **3**, and **5** exhibit a reversible oxidation process; moreover, experimentally these complexes exhibit a i_{pc}/i_{pa} ratio close to unity. Conversely, for complexes **2** and **4** enhanced ΔE_p values are observed, reflecting a more irreversible behavior, while complex **6** is definitely irreversible. The tendency of complexes **2** and **4** to be more irreversible, with respect to **1** and **3**, can be related to their lower thermodynamic stability. Regarding the metal oxidation potential, an expected trend is observed when the electron-withdrawing carboxylate groups are present, reflected in a more difficult $Ru^{2+/3+}$ oxidation for complex **3** (which possesses electron-withdrawing groups, deebpy, in both bpy ligands) compared to **1** and for complex **4** compared to **2**. Specifically, for complexes **1** and **3**, values of 931 and 1115 mV, respectively, are reported. Similarly, complexes **2** and **4** follow the same trend, with $E_{1/2}$ ($Ru^{2+/3+}$) values of 1013 and 1151 mV, respectively. This reflects the expected fact that the bipyridinic ligands with acceptor groups remove electronic density from the ruthenium metallic center, making oxidation of the metal a more energy-demanding process.

The effect of the donor NMe_2 group in the chromophoric ligand on the metal oxidation is less clear. The presence of the donor substituent should make the metal oxidation easier. The experimental trend in Table 2 goes in the opposite direction. Nevertheless, the behavior can be explained by the fact that the ruthenium oxidation occurs on an already positively charged species. Otherwise, it can also be concluded that when both donor and acceptor substituents are present the effect of the latter seems to predominate.

Finally, complexes **5** and **6** can be visualized as originating from the "replacement" in complexes **3** and **4** of a ligand with an acceptor substituent, (bpy-$(COOH)_2$), by a chromophoric ligand. Both facts (the decrease of the number of acceptor ligands and the increase in the number of chromophoric ligands) should tend to make the oxidation easier, and this is clearly observed both in the experimental electrochemical data as well as in the MO calculations.

UV−Vis Spectra Analysis. *1. Ligands.* Absorption spectra of ligands LH and $LNMe_2$ show a broad and intense band centered at 317 and 390 nm, respectively, as can be seen in Figure 4, where results from TDDFT calculations on the gas phase are also displayed. The absorption bands of ligands LH and $LNMe_2$ appear displaced to lower energies when compared to bipyridine (λ_{max} = 280 nm). This red shift has been attributed to the presence of the aromatic π-conjugated system.[31] The effect is enhanced in the $LNMe_2$ ligand, due to the presence of the electron-donating aminoalkyl substituent, Figure 4b. It has also been suggested that these bands correspond to intraligand charge transfer, ILCT, transitions. Addition of a small amount of acid to a solution of the ligand diminishes the intensity of the 380 nm band, probably due to the protonation of the amino group, which, therefore, can no longer participate in the ILCT transition. This experimental test supports the ILCT nature of the bands.

Molecular orbital analysis in terms of the fragment components displayed in Table 3 shows that for the ligand LH the HOMO possesses σ character resulting from the mixing of $p_x + s$ atomic orbitals in the P fragment and that the HOMO−1 and HOMO−2 molecular orbitals possess π character and a more delocalized electronic distribution, with a high contribution of the V and F fragments. On the other hand, the LUMO and LUMO+1 orbitals exhibit π-antibonding character delocalized over the whole molecule, with the main electronic occupancy on the P fragment for the LUMO and V and F fragments for LUMO+1. Finally, LUMO+2 is again dominated by the P fragment. Regarding the $LNMe_2$ ligand, where the dimethylamino substituent has been introduced, the molecular orbital fragment analysis shows, Table 4, that the first three LUMOs are of composition similar to those from the LH ligand. However, a difference is observed in the nature of the HOMO and HOMO−1, where $LNMe_2$ has a composition dominated by the F fragment and a nearly degenerate character for these orbitals.

Additionally, TDDFT calculations were performed, and the results displayed in Table 5. These types of calculations help to obtain insight into the electronic transitions responsible for the absorption spectra. Two main transitions (1A and 1B in Figure 4) having high oscillator strength (0.56 and 0.94, respectively) are responsible for the large absorbance found for ligand LH at 317 nm. Both transitions contain two types of

dx.doi.org/10.1021/ic1020862 |Inorg. Chem. 2011, 50, 5910–5924

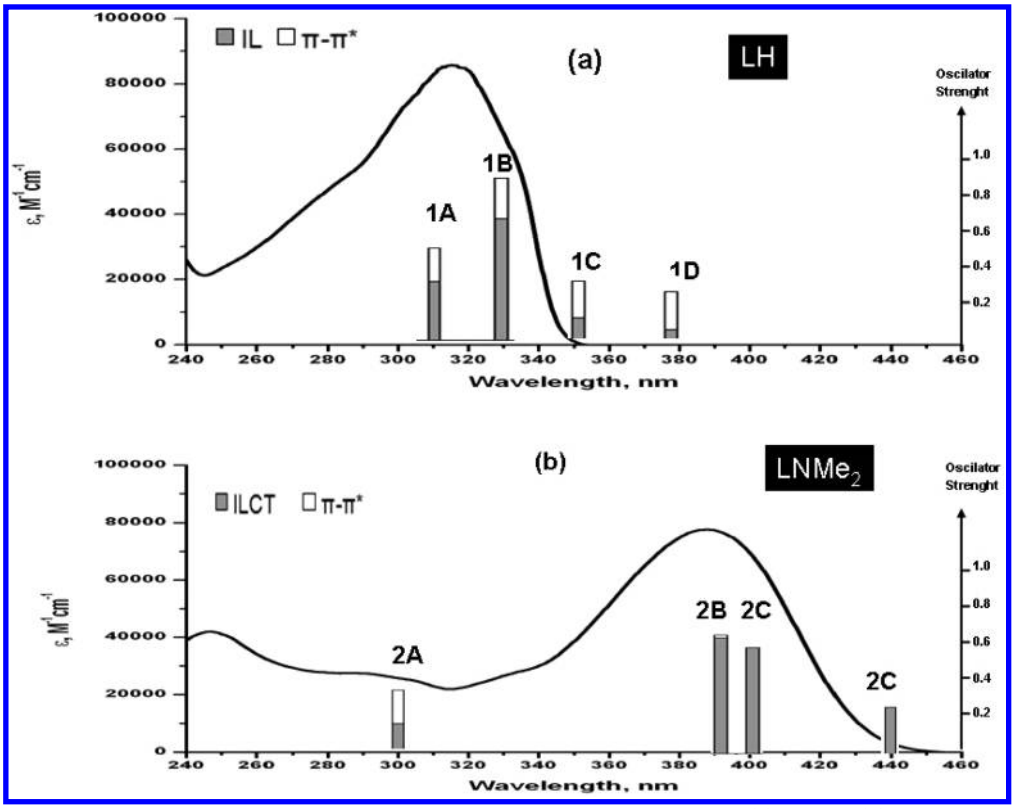

Figure 4. Comparison of UV−vis experimental spectra in CH_3CN with TDDFT results for ligands (a) LH and (b) $LNMe_2$.

Table 3. Decomposition of Molecular Orbitals in Terms of Orthogonal Fragments for LH

			fragment			
MO	occupation	energy	F	V	P	assignment
LUMO+2	0.0	−2.70	9	3	88	π^*(P)
LUMO+1	0.0	−3.28	35	37	28	π^*(F+V)
LUMO	0.0	−3.57	22	28	50	π^*(P)
HOMO	2.0	−6.08	0	0	100	σ(P)
HOMO−1	2.0	−6.22	37	36	27	π(F+V)
HOMO−2	2.0	−6.28	41	36	23	π(F+V)

Table 4. Decomposition of Molecular Orbitals in Terms of Orthogonal Fragments for $LNMe_2$

			fragment			
MO	occupation	energy	F	V	P	assignment
LUMO+2	0.0	−2.04	8	5	87	π^*(P)
LUMO+1	0.0	−2.50	32	37	31	π^*(F+V)
LUMO	0.0	−2.84	20	26	54	π^*(P)
HOMO	2.0	−4.94	70	18	12	π(F)
HOMO−1	2.0	−4.97	71	18	11	π(F)
HOMO−2	2.0	−5.43	0	0	100	σ(P)

excitations: intraligand (IL), which takes place parallel to the molecular axes and involves an electronic displacement from the FV fragment to the P fragment, and $\pi\pi^*$, with an electronic displacement perpendicular to the molecular axes and centered on the π orbital of the FV fragment. Figure 5a shows in a pictorial way an IL excitation, which would be predominant in the mentioned LH bands.

Regarding the $LNMe_2$ ligand, the HOMO and HOMO−1 degenerate molecular orbitals centered in the F fragment participate in transitions 2B and 2C, which result in the red-shifted absorption appearing at 390 nm for the intraligand ILCT transitions from fragment F to fragment P, Figure 5c.

2. Complexes. The absorption spectra for the ruthenium complexes studied in this work show two characteristic bands: The first one appears in the UV region and shows high ε values. This band can be associated with the absorbance of the chromophoric ligand due to its similarity to the band appearing in the absorption spectra of the uncoordinated ligands, although red shifted due to the effect of coordination to the metallic center. The second broad and less intense band is located in the visible region and, according to literature,[32] is mainly assigned as a MLCT band, considering also the fact that it appears at lower energy. Regarding solar cell devices, the second band is more relevant in the injection process and therefore is interesting to analyze. Also, since the energy absorbed comes from the visible region, it could be expected that modifications of the structure of the complexes will result in a change of the energy and intensity of the band, giving rise to an improvement of the solar cell device. In order to gain more insight into the composition of this broad band, a transition density analysis (TDA), coupled with a TDDFT calculation, was performed over the series of complexes under study, in a similar way to that done for the ligands. However, for the case of the complexes, molecular orbitals were decomposed in five basic fragments containing ruthenium, bipyridine, and the three F, V, P fragments coming from the chromophoric ligands. According to this and considering the

dx.doi.org/10.1021/ic1020862 |*Inorg. Chem.* 2011, 50, 5910–5924

Table 5. Assignment of the Main Contributing Transitions to the Overall Absorption Bands in LH and $LNMe_2$

ligand	transition	wavelength (nm)	oscillator strength	fragments involved	assignment
LH	1A	311	0.56	FV → P + FV → FV	IL + $\pi\pi^*$
	1B	329	0.94	FV → P + FV → FV	IL + $\pi\pi^*$
$LNMe_2$	2B	386	0.63	F → P	ILCT
	2C	403	0.53	F → P	ILCT

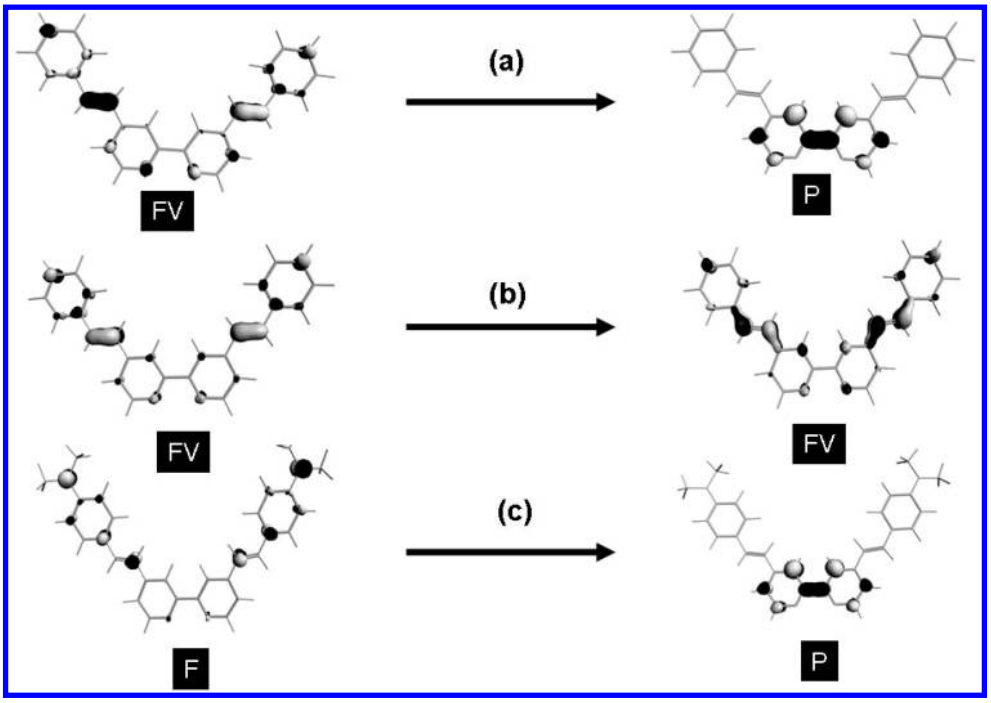

Figure 5. Example of electronic transitions in free ligands involving two molecular orbitals described in terms of orthogonal fragments: (a) intraligand (IL); (b) $\pi \rightarrow \pi^*$; (c) intraligand charge transfer (ILCT). Note that ILCT bands imply a remarkable charge displacement from one region of the ligand to another, with a consequent change in dipolar moment.

predominance of each fragment in the overall composition, molecular orbitals can be classified as centered on the metal, centered on the chromophoric ligand, or centered on the bipyridine or mixtures between them. On the other hand, the TDA method shows that each transition is composed by a sum of the single electronic transitions that link an occupied MO from the ground state (GS) with a corresponding MO from the excited state (ES). Employing the above classification of the MO it is possible to distinguish four basic types of electronic transitions, which are depicted in Figure 6. Electronic transitions a and b belong to the category of metal-to-ligand charge transfer, MLCT, and involve a charge transfer from the ruthenium atom to the chromophoric ligand (MC) or to bipyridine (MB). The ligand to ligand (LL) transition, shown in c, corresponds to a charge transfer between the F-substituted fragment of the chromophoric ligand and bipyridine. Finally, Figure 6d shows a charge transfer process that occurs inside the chromophoric $LNMe_2$ ligand, which is classified as an intraligand process (ILCT).[32] If the intraligand process does not show clear charge transfer character, it is named as IL, as would be the case of complexes with the LH ligand.

Figure 7 shows the experimental spectra for complexes **3**−**6** as well as the single transitions calculated by TDDFT in terms of stacked columns representing the contribution of each of the four basic electronic transitions to the overall absorption band. Furthermore, the total height of each column corresponds to the oscillator strength of the corresponding transition. Hence, in this way it is easy to determine how the calculated transitions influence the shape and maxima of the experimental band.

According to Figure 7, the spectra of complex **3** with λ_{max} = 473 nm and ε_{max} = 24 000 M^{-1} cm^{-1} contain seven main transitions located within the range from 410 to 580 nm. Transition 3D occurs at 457 nm, has the highest oscillator strength (0.29), and contains mainly an IL electron transfer process. The metal to bipyridine electron transfer (MB) can be found contributing to transitions 3C (449 nm), 3E (461 nm), and 3F (484 nm), although for the latter two the MB process is coupled with IL and LL basic transitions. When the number of "chromophoric ligands" present in the complex is increased, as is the case of complex **5** with respect to **3**, the extinction molar coefficient increases from 24 000 to 35 000 $M^{-1}cm^{-1}$. The simulated spectrum of **5** shows, in the range from 450 to 550 nm, an increase in the number of transitions corresponding to MLCT bands. Moreover, transition 5J, located at 494 nm and showing the highest oscillator strength (0.19), is close to λ_{max}. The reduced contribution of IL and LL basic transitions to the overall absorption of this complex is noteworthy. On the other hand, the presence of the dimethylamino substituent on the chromophoric ligand ($LNMe_2$ ligand) produces a significant increase in the ε value, as is the case of complex **4**, with a ε_{max} of

dx.doi.org/10.1021/ic1020862 |*Inorg. Chem.* 2011, 50, 5910–5924

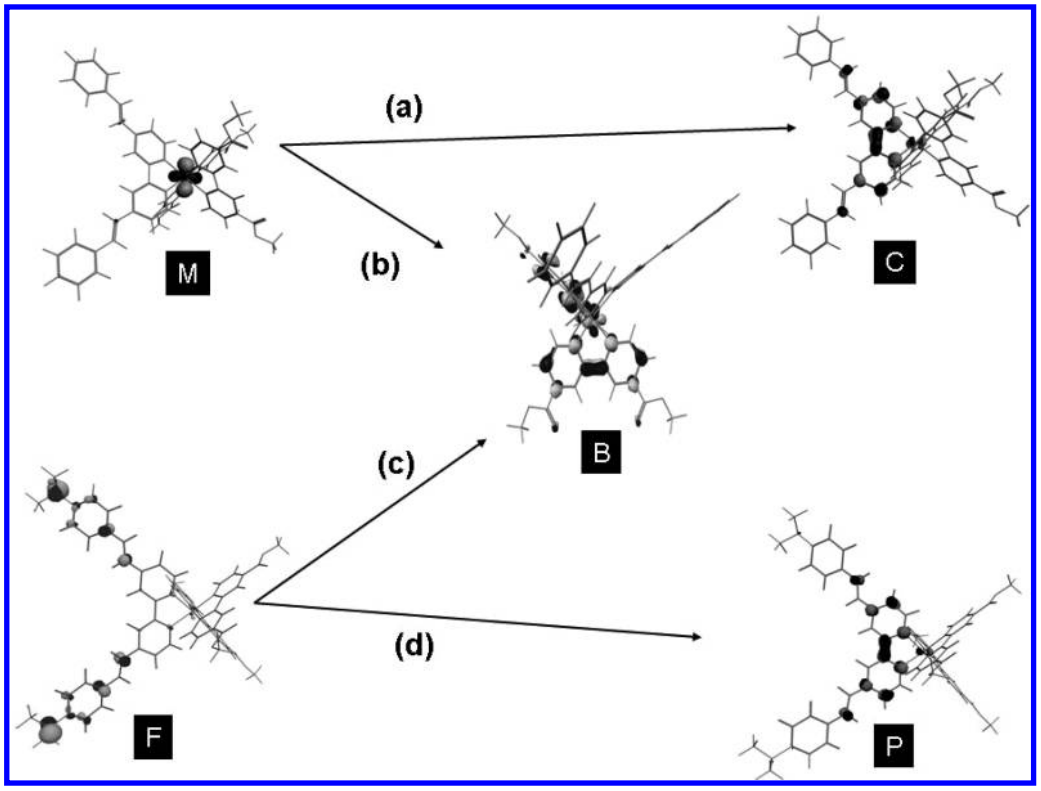

Figure 6. Example of basic electronic transitions in ruthenium complexes involving two molecular orbitals described in terms of orthogonal fragments: (a) MC = metal to chromophoric ligand charge transfer; (b) MB = metal to bipyridine ligand charge transfer; (c) LL = interligand transfer from chromophore to bipyridine; (d) ILCT = intraligand charge transfer.

46 800 $M^{-1}cm^{-1}$, compared to 24 000 $M^{-1}cm^{-1}$ of complex **3**. The TDDFT calculations show the appearance of two very intense transitions, 4F and 4G, located at 479 and 489 nm with oscillator strengths of 0.46 and 0.42, respectively. Both 4F and 4G are composed by a mixture of MB, LL, and ILCT electronic transitions, with predominance of the latter. Transitions 4J and 4K, mainly composed of ILCT and LL transitions, are responsible for the increase of the absorbance on the tail of the band and the enhancement of its width up to 570 nm. On the other hand, complex **6**, with two chromophoric $LNMe_2$ ligands, exhibits an increase of the extinction molar coefficient up to 67 000 M^{-1} cm^{-1} and the appearance of a maximum at 426 nm. Theoretical analysis reveals an increase in the number of transitions to be considered (from 8 to 11) and the presence of two transitions located at 407 (6A) and 524 nm (6I) with oscillator strengths of 0.26 and 0.79, respectively. The 6A transition is mainly a MLCT electron transition from ruthenium to the chromophoric ligand, while 6H and the neighboring bands 6J, 6I, and 6 L evidence a predominance of ILCT character.

The overall contribution of the four basic electronic transitions in the absorption region comprised between 400 and 600 nm for the series of complexes under study is displayed in Figure 8. As can be seen, each complex possesses a characteristic pattern determined by the acceptor−donor character of the substituents on both ligands. For the unsubstituted model complex **1** the absorption band is composed mainly by intraligand (IL) and metal to chromophoric ligand (MC) processes. When an electron-attracting substituent, such as −COOMe, is attached to the bipyridine ligand (complex **3**), an enhancement of the electronic transfer between metal to bipyridine (MB) occurs at the expense of the metal to chromophore electronic transitions. On the other hand, when two chromophoric ligands are present (complex **5**) a predominance of the metal to chromophore transition is observed. Taking again as reference the model complex **1**, introduction of the donor amino substituent in the chromophore, as in **2**, causes a detrimental effect over MC transitions and favors LL and MB transitions. Attaching the methyl ester electron-acceptor substituent, as in **4**, results mainly in the enhancement of metal to bipyridine charge transfer transitions. The intraligand charge transfer process (ILCT) is noticeably favored when two electron-donor-substituted chromophoric ligands are present, as in **6**, in accordance with previous reports.[12]

By combining the results from Figures 7 and 8, it is possible to build a simple theoretical model predicting the behavior of such complexes when employed as dyes in solar cell devices. The white column in Figure 9 represents the total energy absorbed (E_A) by the complexes in the range from 0.113 to 0.076 eV (400−600 nm). This value is calculated through the product $f_{max}\Delta\nu$, eq 6, which is proportional to the area under the curve of the experimental absorption spectra (f_{max} is the highest oscillator strength value obtained from TDDFT). From this figure it can be seen that, as expected, the amount of energy absorbed is correlated with the number of chromophoric ligands present in the complex. On the other hand, the increase in absorbed energy is evident when chromophoric ligands with dimethylamino substituents are present in the complex, as in **4** and **6**, when compared to **3** and **5**, respectively. Additionally, the black and striped columns in Figure 9 show the amount of absorbed energy delivered to the bypiridinic, E_D(B), and chromophoric, E_D(C), ligands by means of (MB + LL) and MC absorption

dx.doi.org/10.1021/ic1020862 |*Inorg. Chem.* 2011, 50, 5910–5924

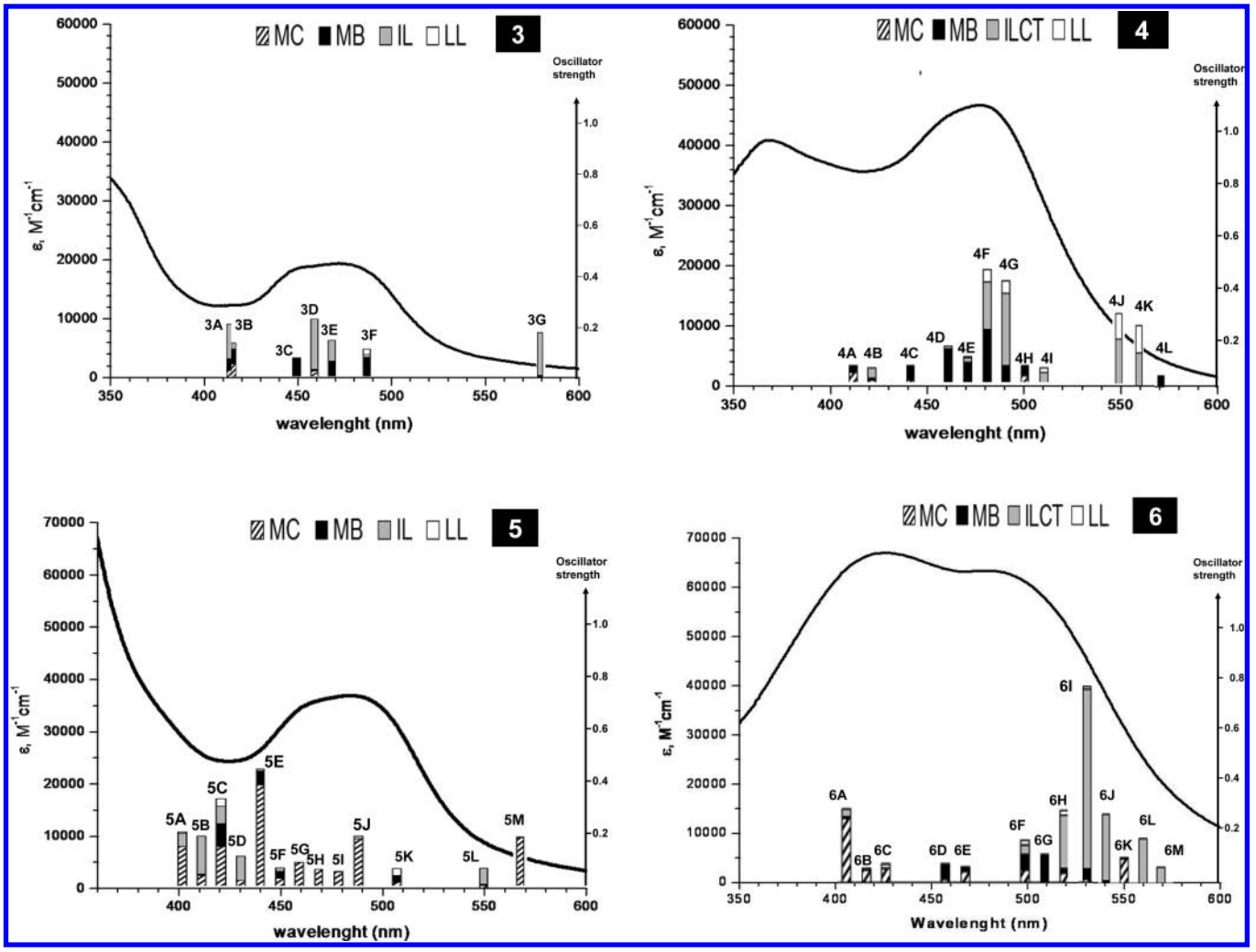

Figure 7. Comparison of UV−vis experimental spectra in CH_3CN with TDDFT results (Γ_λ function of eq 3) for the ligands in complexes **3**−**6**.

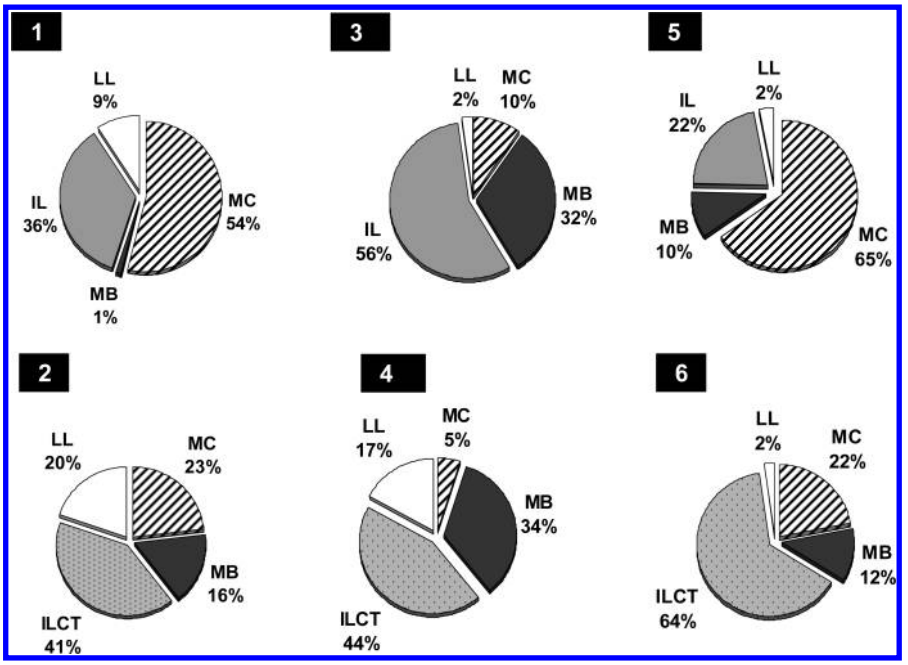

Figure 8. Distribution function, $\zeta(\alpha,\beta)$ in eq 4, of the four basic types of electronic transitions along the visible band (400−600 nm) for complexes **1**−**6**.

dx.doi.org/10.1021/ic1020862 |*Inorg. Chem.* 2011, 50, 5910–5924

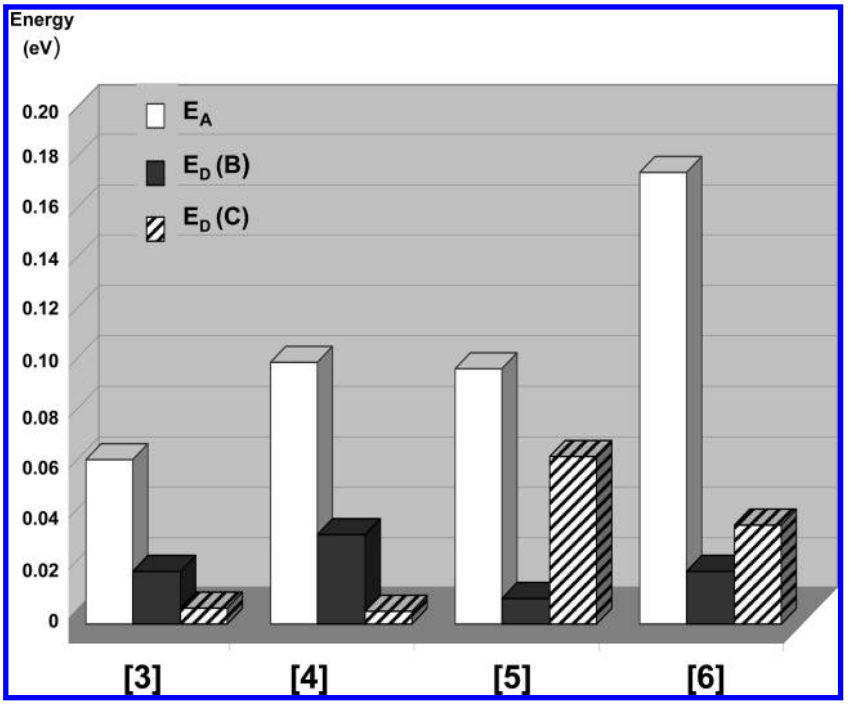

Figure 9. Available energy for electronic injection; E_A = absorbed energy, $E_D(B)$ = energy delivered to bipyridine, $E_D(C)$ = energy delivered to the chromophoric ligand.

processes, respectively. For an efficient direct electronic injection, most of the absorbed energy should be transferred to the ligand anchored on the semiconductor surface. However, inspection of Figure 9 shows that the greater amount of absorbed energy (white column) in **5** and **6**, with respect to **3**, does not necessarily mean an increase in the amount of direct electronic injection capacity (black column). From the E_D/E_A ratio (Tables S3−S6 in the Supporting Information) it can be estimated that for complexes **5** and **6** a maximum of 14% of the absorbed energy is available for injection (i.e., only 14% of the electronic density after excitation is concentrated on the anchoring ligand), compared with the 51% available for **4** and 34% for **3**.

Emission and Triplet State. The chromophoric LH and $LNMe_2$ ligands have an emission band in acetonitrile at room temperature. Table 6 summarizes the relevant emission data for these ligands and their corresponding complexes. Complexes **1**, **2**, **3**, and **5** have emission processes in acetonitrile at room temperature in the absence of oxygen. It should be mentioned that the electrochemical data of Table 2, specifically the difference Δ between the first reduction and the first oxidation potentials, show a good correlation with the emission results. For example, the Δ value diminishes from 2.35 to 2.26 V on going from **3** to **5** while E_{EM} decreases from 1.97 to 1.87 eV.

It is noteworthy that the emission energy of **2** is close to the value reported for a similar complex containing only one dimethylamino styryl substituent on the bpy fragment, instead of two as in LH.[31] Although in this case, dual emission was reported; the dimethylamino styryl ligand was found to emit at 1.82 eV. This value suggests that emission of **2** arises mainly from the chromophoric ligand. It should also be mentioned that the presence of COOMe groups as substituents on bipyridine, as in **4** and **6**, seems to be detrimental for the emission since in both complexes no emission is observed. This can be due either to the predominance of nonradiative deactivation pathways or to a sort of quenching process by the ester group.

Table 6. Spectroscopic Data for Ligands and Complexes

compound	λ_{max}(Abs)[a] (nm)		ε (M^{-1} cm^{-1})	λ_{max}(Em)[b] (nm)
LH	317	ILCT		376
$LNMe_2$	390	ILCT		520
1	465	MLCT	22 300	642
	326	ILCT	46 200	
2	468	MLCT	46 900	673
	410	ILCT-ML	42 000	
3	473	MLCT	24 000	629
	349	ILCT	43 500	
4	477	MLCT	46 800	
	370	ILCT	40 900	
5	486	MLCT	35 000	664
	329	ILCT	92 000	
6	480	MLCT	63 400	
	426	ILCT	67 000	

[a] Solvent: CH_3CN, [b] Determined at room temperature in CH_3CN.

At this point it is relevant to mention that the injection process analysis made in the previous sections of this work has been focused mainly on two aspects: (1) the fraction of light absorbed through Franck−Condon (FC) transitions that is available for charge injection (eq 4) and (2) the fraction of excitation energy that is ultimately localized on the ligand that is bound to the semiconductor surface by means of the anchoring carboxy group (eq 5). However, it is important to consider that from an experimental point of view, although it is possible that hot vibrational (essentially FC) states contribute to charge injection, this process occurs mainly from the thermally equilibrated (thexi)

dx.doi.org/10.1021/ic1020862 |Inorg. Chem. 2011, 50, 5910–5924

Table 7. Distribution Function $\varphi_T(g_\beta)$ for the HSOMO Orbital, and Orbital Energetic for the Triplet State of Complexes 1−6[a]

				φ_T		
complex	E_{EM}	E_T[b]	I_T(bpy)[c]	L	Ru	bpy
$Ru(bpy)_3^{+2}$	2.07	2.30				100 (100)
1	1.93	1.57		77 (95)	2 (5)	21 (0)
2	1.84	1.06		63 (0)	0 (3)	37 (97)
3	1.97	1.76	0.012	36 (3)	0 (2)	64 (95)
4		0.88	0.026	24 (1)	0 (2)	76 (97)
5	1.87	1.54	0.004	56 (2)	1 (4)	43 (94)
6		1.04	0.011	45 (0)	0 (6)	55 (94)

[a] L = chromophoric ligand, LH or $LNMe_2$, Bpy = bipyridine or dicarboxybipyridine. Values for the singlet state through LUMO composition are displayed in parentheses for comparison purposes. All energies in eV. [b] $E_T = E(T_0) - E(T_1)$. [c] I_T(bpy) = available energy to be injected from the bpy fragment on the T_1 state (eq 7).

excited state. For ruthenium polypyridinic-type complexes, the triplet state is a good candidate for the mentioned thexi state.

Therefore, optimization of the triplet state for the series of compounds under study was performed. Table 7 displays calculated triplet energies, indicated as E_T. The values were obtained from the difference between the total energy of the optimized triplet state and the total energy of the ground singlet state, calculated in the triplet state optimized geometry. Available data for $Ru(bpy)_3^{+2}$ was included for comparison reasons. A linear correlation coefficient of 0.95 was found when comparing experimental emission data, E_{EM}, with theoretical E_T values. In accordance with this, the trend of the experimental emission energy is correctly reproduced by the calculated values: **3** > **1** > **5** > **2**. It is also predicted that complex **2** shows a lower emission energy along the series under study as well as that NMe_2 substitution shifts the emission band to lower energy regions.

From another point of view, the composition of the highest spin occupied molecular orbital (HSOMO) can be analyzed in terms of molecular fragments, Table 7. Through a first examination, it can be seen that the triplet states are mostly characterized by an increase in the participation of the chromophoric ligand when compared to its contribution in the corresponding singlet state (in parentheses in Table 7). More important, the chromophoric ligand becomes the predominant fragment in complexes **2** and **5**, where no contribution of this fragment was observed in the singlet state. This effect can also be detected when two chromophores are present, as can be observed on comparing complexes **3** and **5**, where an increase of 19% in the contribution of this fragment is observed in the latter, while a comparison of complexes **4** and **6** shows that this increase corresponds to 20%. Note that on comparing **3** and **5** the nature of the triplet state is quite different since in the former it is located on the bpy fragment while for the latter it is found on the chromophore. This difference can be related to the emission spectral shift from 629 to 664 nm.

To understand the role of this triplet state with regard to electronic injection efficiency, it is necessary to use eq 7 to calculate I_T(bpy) in relation to the bpy fragment, i.e., the fragment that contains the anchoring COOMe groups and therefore has the possibility of direct injection of the electrons in the semiconductor

$$I_T(\text{bpy}) = E(\text{bpy})\varphi_T(\text{bpy}) \quad (8)$$

E(bpy) is obtained from eq 5, and values for φ_T(bpy) are obtained through the last column of Table 7. It can be seen in this table that, as expected, complexes possessing two bpy ligands (**4**, **3**) exhibit higher values for φ_T(bpy) than those with only one (**5**, **6**). Moreover, electron-withdrawing substituents, such as COOMe, increase the values of φ_T(bpy), as can be seen by comparing **4** and **3** with **1** and **2**.

Results obtained for eq 8 are displayed in the fourth column of Table 7. It can be seen that complex **4** shows the highest value for the bpy fragment in I_T followed by **3**. This result coincides with the tendency previously found for the Franck−Condon singlet in Figure 9.

REMARKS AND CONCLUSIONS

As discussed in the text, an understanding of the spectroscopic and electrochemical properties of the complexes could be made with the help of theoretical calculations. This was achieved mainly by comparing the relative energy and composition of the MOs involved and the nature of the electronic transitions associated to each absorption and emission band for the different complexes.

As mentioned in the Introduction and in the cited literature therein, ruthenium complexes bearing chromophoric ligands should be a good choice as solar cell dyes due to the fact that these ligands considerably increase the molar extinction coefficient values, which are directly related to the light absorbance or light-harvesting efficiency (LHE). Taking into account the fact that the major aim of this article is to elucidate if the absorbed photons by this variety of dyes with chromophoric ligands are potentially useful in the generation of electric current, the results here reported allow one to conclude that not necessarily all the transitions involved in the absorption bands will end in an effective one-electron injection process to the semiconductor conduction band. Therefore, an increase in LHE not necessarily should imply an increase in IPCE. This general conclusion is based on the following facts:

1 As can be seen in Table 6, when a donor group, such as NMe_2, is introduced in the chromophoric ligand, as in complexes **4** and **6**, an enhancement of the molar extinction coefficient is observed for the lowest energy band, increasing therefore its visible light-harvesting capacity. Nevertheless, according to Figure 8, a predominance of LL or ILCT intraligand bands is observed for these complexes, limiting their possibilities as dyes, as these types of absorptions lack the directionality of MLCT bands.

2 Figure 8 gives the composition of the whole visible absorption framework for the different complexes in terms of the basic transitions described in Figure 6. It can be seen that complex **5** shows the highest contribution of MC absorption and therefore is very efficient in light harvesting, as reflected by its high molar extinction coefficient. However, complexes **3** and **4** possess the highest contribution of MB transitions of all the complexes in the series studied, Figure 8, making a direct injection processes more feasible in these complexes. In fact, MB transitions involve an electronic transition to the ligand, which would be anchored to the semiconductor in a solar cell.

dx.doi.org/10.1021/ic1020862 |*Inorg. Chem.* 2011, 50, 5910–5924

3 A comparison of **3** with **5** permits one to establish that introduction of a second chromophoric ligand diminishes the MB contribution of the band. The same is true when comparing **4** and **6**.
4 From remarks 2 and 3 it follows that although chromophoric groups and donor substituents on the ligands are good options to increase light-harvesting efficiency (LHE), their possible contribution to an efficient IPCE must be analyzed from the point of view of their contribution to the generation of excited states potentially useful for direct injection.
5 According to Figure 9 it can be expected that complexes **3** and **4** are most suitable to be employed as sensitizers on a solar cell design. In fact, although complex **6** is the one with the highest absorption and while complex **5** absorbs similar to complex **4**, they have a lower amount of available energy for injection, as described above. It must also be considered that according to Figure 8 complex **4** has the highest contribution to LL (LH → bpy) bands, a fact that could increase the electron density on the ligand where direct injection arises.
6 According to Table 7, when considering electronic injection coming from the first triplet excited state, the calculated amount of energy that can be injected suggests that complexes **3** and **4** are the most suitable, in accordance with the above discussion.

It must be finally pointed out that the previous analysis was centered on direct electron injection. Nevertheless, in a cell, through-space electronic injection could also be observed;[33] if this is the case, the contribution of MC absorptions to the IPCE would become more relevant.

■ ASSOCIATED CONTENT

Supporting Information. Comparison of calculated and experimental UV−vis spectra for complex **3** using different exchange-correlation functions, Figure S1, frontier orbital energy and population, and percent of contribution of each basic excitation to the electronic transition for complexes **1**−**6**, Tables S1−S6, and Cartesian coordinates for the optimized ground and triplet states for compounds **1**−**6**, Tables S7−S12 and S13−S18, respectively. This material is available free of charge via the Internet at http://pubs.acs.org.

■ AUTHOR INFORMATION

Corresponding Author
*E-mail: bloeb@puc.cl.

■ ACKNOWLEDGMENT

FONDECYT Grant 1070799 is gratefully acknowledged. We would also like to acknowledge Dr. Ramiro Arratia-Perez from UNAB for his kind support in regard to calculation facilities.

■ REFERENCES

(1) (a) Altobello, S.; Argazzi, R.; Caramori, S.; Contado, C.; Da Fré, S.; Rubino, P.; Choné, C.; Larramona, G.; Bignozzi, C. A. *J. Am. Chem. Soc.* **2005**, *127*, 15342. (b) Nazeeruddin, M. K.; Kay, A.; Rodicio, I.; Humphry-Baker, R.; Müller, E.; Liska, P.; Vlachopoulos, N.; Grätzel, M. *J. Am. Chem. Soc.* **1993**, *115*, 6382. (c) Kelly, C. A.; Farzad, F.; Thompson, D. W.; Stipkala, J. M.; Meyer, G. J. *Langmuir* **1999**, *15*, 7047. (d) Kuang, D.; Klein, C.; Ito, S.; Moser, J.-E.; Humphry-Baker, R.; Zakeeruddin, S. M.; Grätzel, M. *Adv. Funct. Mater.* **2007**, *17*, 154. (e) Nazeeruddin, M. K.; Péchy, P.; Renouard, T.; Zakeeruddin, S. M.; Humphry-Baker, R.; Comte, P.; Liska, P.; Cevey, L.; Costa, E.; Shklover, V.; Spiccia, L.; Deacon, G. B.; Bignozzi, C. A.; Grätzel, M. *J. Am. Chem. Soc.* **2001**, *123*, 1613. (f) Wang, Z.-S.; Yamaguchi, T.; Sugihara, H.; Arakawa, H. *Langmuir* **2005**, *21*, 4272.

(2) (a) Le Bouder, T.; Viau., L.; Guégan, J.-P.; Maury, O.; Le Bozec, H. *Eur. J. Org. Chem.* **2002**, 3024. (b) Viau, L.; Malkowsky, I.; Costuas, K.; Boulin, S.; Toupet, L.; Ishow, E.; Nakatani, K.; Maury, O.; Le Bozec, H. *Chem. Phys. Chem.* **2006**, *7*, 644. (c) Hagfeld, A.; Gtzel, M. *Chem. Rev.* **1995**, *95*, 49. (d) Wang, P.; Klein, C.; Humphry-Baker, R.; Zakeeruddin, S. M.; Grätzel, M. *J. Am. Chem. Soc.* **2005**, *127*, 808.

(3) Meyer, G. J. *J. Chem. Educ.* **1997**, *74*, 652.

(4) Jiang, K.-J.; Xia, J.-B.; Masaki, N.; Shuji, N.; Yanagida, S. *Inorg. Chem.* **2008**, *361*, 783.

(5) (a) Aranyos, V.; Hjelm, J.; Hagfeldt, A.; Grennberg, H. *Dalton Trans* **2003**, 1280. (b) Jang, S.-R.; Lee, C.; Choi, H.; Ko, J. J.; Lee, J.; Vittal, R.; Kim, K.-J. *Chem. Mater.* **2006**, *18*, 5604. (c) Handa, S.; Wietasch, H.; Thelakkat, M.; Durranta, J. R.; Haque, S. A. *Chem. Commun.* **2007**, *17*, 1725.

(6) Renouard, T.; Le Bozec, H.; Brasselet, S.; Ledoux, I.; Zyss, J. *Chem. Commun.* **1999**, 871.

(7) Le Bouder, T.; Maury, O.; Bondon, O.; Costuas, K.; Amouyal, E.; Ledoux, I.; Zyss, J.; Le Bozec, H. *J. Am. Chem. Soc.* **2003**, *125*, 12284.

(8) (a) Nazeeruddin, M. K.; Wang, Q.; Cevey, L.; Aranyos, V.; Liska, P.; Figgemeier, E.; Klein, C.; Hirata, N.; Koops, S.; Haque, S. A.; Durrant, J. R.; Hagfeldt, A.; Lever, A. B. P.; Grätzel, M. *Inorg. Chem.* **2006**, *45*, 787. (b) Angelis, F. D.; Fantacci, S.; Selloni, A.; Grätzel, M.; Nazeeruddin, M. K. *Nano Lett.* **2007**, *7*, 3189.

(9) Snaith, H. J.; Karthikeyan, C. S.; Petrozza., A.; Teuscher, J.; Moser, J. E.; Nazeeruddin, M. K.; Thelakkat, M.; Grätzel, M. *J. Phys. Chem. C* **2008**, *112*, 7562.

(10) (a) Wang, P.; Zakeeruddin, S. M.; Moser, J. E.; Humphry-Baker, R.; Comte, P.; Aranyos, V.; Hagfeldt, A.; Nazeerunddin, M. K.; Grätzel, M. *Adv. Mater.* **2004**, *16*, 1806. (b) Wang., P.; Zakeeruddin, S. M.; Moser, J. E.; Nazeeruddin, M.; Sekiguchi, T.; Grätzel, M. *Nat. Mater.* **2003**, *2*, 402.

(11) Beer, P. D.; Kocian., O.; Mortimer, R. J.; Ridgway, C. *J. Chem. Soc., Dalton Trans.* **1993**, 2629.

(12) Cook, M. J.; Lewis, A. P.; McAuliffe, G. S. G.; Skarda, V.; Thomson, A. J.; Glasper, J. L.; Robbins, D. J. *J. Chem. Soc., Perkin Trans II* **1984**, 1293.

(13) (a) Karthikeyan, C. S.; Peter, K.; Wietasch, H.; Thelakkat, M. *Sol. Energy Mater. Sol. Cells* **2007**, *91*, 432. (b) Perez, L. C.; Kador, L.; Peng, B.; Thelakkat, M. *J. Phys. Chem. B* **2005**, *109*, 5783.

(14) Donnici, C. L.; Máximo, F. D. H.; Cruz, M.; Teixeira, L. L.; dos Reis, G.; Santos, C. E.; Ferreira de Oliveira, I. M.; Carvalho, S.; Paniago, E. B. *J. Braz. Chem. Soc.* **1998**, *9*, 455.

(15) Zhou, M.; Robertson, G. P.; Roovers, J. *Inorg. Chem.* **2005**, *44*, 8317.

(16) Sullivan, B. P.; Salmon, D. J.; Meyer, T. J. *Inorg. Chem.* **1978**, *17*, 3334.

(17) Velde, G.; Bickelhaupt, F. M.; Van Gisbergen, S. J. A.; Fonseca Guerra, C.; Baerends, E. J.; Snijders, J. G.; Ziegler, T. *J. Comput. Chem.* **2002**, *22*, 931.

(18) Perdew, J. P.; Wang, Y. *Phys. Rev. B* **1992**, *45*, 13244.

(19) Vosko, S. H.; Wilk, L.; Nusair, M. *Can. J. Phys.* **1980**, *58*, 1200.

(20) Becke, A. D. *Phys. Rev. B* **1986**, *34*, 7406.

(21) Van Lenthe, E.; Baerends, E. J. *J. Comput. Chem.* **2003**, *24*, 1142.

(22) Perdew, J. P.; Burke, K.; Ernzerhof, M. *Phys. Rev. Lett.* **1996**, *77*, 3865.

(23) (a) Handy, N. C.; Cohen, A. J. *Mol. Phys.* **2001**, *99*, 403. (b) Lee, C.; Yang, W.; Parr, R. G. *Phys. Rev. B* **1988**, *37*, 785.

(24) Van Leeuwen, R.; Baerends, E. J. *Phys. Rev. A* **1994**, *49*, 2421.

(25) (a) Hirshfeld, F. L. *Theor. Chim. Acta* **1977**, *44*, 129. (b) Wiberg, K. B.; Rablen, P. R. *J. Comput. Chem.* **1993**, *44*, 1504.

(26) Juris, A.; Campagna, S.; Bidd, I; Lehn, I.-B.; Ziessel, R. *Inorg. Chem.* **1988**, *27*, 4007.

(27) Leidner, C. R.; Sullivan, B. P.; Reed, R. A; White, B. A.; Crimmins, M. T.; Murray, R. W.; Meyer, T. J. *Inorg. Chem.* **1987**, *26*, 882.
(28) Kohn, W.; Sham, L. J. *Phys Rev* . **1965**, *140*, A1133.
(29) Almbladth, C.; Von Barth, U. *Phys. Rev. B* **1985**, *31*, 3231.
(30) (a) Barrera, M.; Zuloaga, F. *Int. J. Quantum Chem.* **2006**, *106*, 2044. (b) Barrera, M.; Zuloaga, F. *J. Chil. Chem. Soc.* **2003**, *4*, 27. (c) Goycolea, C.; Barrera, M.; Zuloaga, F. *Int. J. Quantum Chem.* **1989**, *54*, 123.
(31) Song, L.-G.; Feng, J.; Wang, X.-S.; Yu, J.-H.; Hou, Y.-J.; Xie, P.-H.; Zhang, B.-W.; Xiang, J.-F.; Ai, X.-C.; Zhang, J.-P. *Inorg. Chem.* **2003**, *42*, 3393.
(32) Han, X.; Wu, L.-Z.; Si, G.; Pan, J.; Yang, Q.-Z.; Zhang, L.-P.; Tung, C.-H. *Chem.—Eur. J.* **2007**, *13*, 1231.
(33) Gajardo, F.; Leiva, A. M.; Loeb, B.; Delgadillo, A.; Stromberg, J. R.; Meyer, G. J. *Inorg. Chem. Acta* **2008**, *361*, 613.

NOTE ADDED AFTER ASAP PUBLICATION

This paper was published on the Web on May 31, 2011. Due to a production error, Figure 2 is incorrect. The corrected version was reposted on June 6, 2011.